Hindawi
Journal of Sensors
Volume 2024, Article ID 8551009, 13 pages
https://doi.org/10.1155/2024/8551009

Research Article

Fault Feature Extraction Method of Rolling Bearing Based on IAFD and TKEO

Kai Guo,[1,2] Jun Ma,[1,2] Xin Xiong,[1,2] Yuming Hu,[1,2] and Xiang Li[1,2]

[1]*Faculty of Information Engineering and Automation, Kunming University of Science and Technology, Kunming 650500, China*
[2]*Yunnan Key Laboratory of Artificial Intelligence, Kunming University of Science and Technology, Kunming 650500, China*

Correspondence should be addressed to Jun Ma; mjun@kust.edu.cn

Received 2 March 2023; Revised 7 January 2024; Accepted 12 January 2024; Published 15 February 2024

Academic Editor: Nageswara Lalam

The study of bearing fault feature extraction using adaptive Fourier decomposition (AFD) holds significant practical importance. However, AFD is constrained by its reliance on prior knowledge for determining decomposition levels, which can result in either underdecomposition or overdecomposition based on a single indicator. Consequently, an improved adaptive Fourier decomposition (IAFD) is proposed. First, a combined weight index called SP is constructed, and the whale optimization algorithm is employed to optimize the SP weight parameter. Second, the IAFD decomposition levels can be adaptively determined using the optimized SP. Finally, a feature extraction method-based IAFD and Teager–Kaiser energy operator is applied in rolling bearing fault diagnosis. Case studies on the Case Western Reserve University and self-made KUST-SY datasets validate the effectiveness of the proposed method.

1. Introduction

Rolling bearing is one of the essential components in rotating mechanical equipment [1], which is widely used in aerospace, trains, wind turbines, and other equipment, and its failure will lead to the decline of equipment performance, resulting in huge safety accidents and economic losses [2]. Therefore, extracting the fault characteristics of rolling bearings is of great significance for the timely and effective determination of their working conditions and for ensuring production safety [3].

Existing bearing fault diagnosis techniques mainly include the vibration signal analysis method, acoustic emission method, oil contamination analysis method, and so on. However, the vibration signal of the bearing shows nonstationary and nonlinear characteristics [4]. At present, the fault feature extraction methods based on an adaptive decomposition of vibration signals have attracted more and more attention [5]. Among them, the most representative decomposition method is the empirical mode decomposition (EMD) method, which can adaptively decompose the vibration signal into several intrinsic mode functions and has been widely used in engineering [6–8]. However, using the cubic spline method to construct the mean curve, EMD may suffer from overenvelopment, underenvelopment, and poor envelope fitting accuracy [9].To improve the accuracy of envelope fitting and the problem of overenvelope and underenvelope, Smith proposed the local mean decomposition (LMD) method, in which a single-component AM-FM signal is viewed as the product of its own envelope signal and a pure FM signal. The complete time–frequency distribution can be obtained by performing a frequency-domain analysis of the PF component [10]. The LMD decomposition method retains more localized information than EMD, which improves the envelope fitting accuracy to some extent and solves the overenvelope and underenvelope problems to a certain extent [11]. However, the components obtained by the LMD often have many spurious frequencies, which can cause abrupt signal changes and high computational effort [12]. Inspired by EMD and LMD, Cheng et al. [13] proposed a new nonsmooth, nonlinear adaptive decomposition method, local characteristic-scale decomposition (LCD). The LCD can decompose a complex signal into the sum of several intrinsic scale components with the physical meaning of instantaneous frequency [14]. Compared with EMD and LMD methods, LCD not only greatly

improves the calculation speed but also effectively suppresses the overenvelope and underenvelope and reduces the fitting error. However, the key to the LCD method lies in the construction of the mean curve based on a linear transformation of the signal itself, which results in distortion due to burrs in the waveforms of the decomposed components [15]. Therefore, how to effectively characterize the fault characteristics of rolling bearings becomes particularly important.

To realize adaptive signal decomposition, Qian et al. [16] proposed a new signal decomposition method, namely the adaptive Fourier decomposition (AFD) algorithm. AFD preserves the vibrational characteristics of the original signal by using an adaptive basis function and the energy distribution of the signal to decompose the signal into elementary segments containing only positive frequencies and selecting the effective components according to the principle of energy maximization. Therefore, its decomposition components not only have good convergence but also follow the energy extraction from high to low, which is suitable for nonsmooth and nonlinear signal analysis. Wang et al. [17] applied the AFD algorithm to ECG signal denoising and verified the effectiveness of AFD by testing the arrhythmia database. Because of the spectral overlap and mutual interference between lung sounds and heart sounds, Wang et al. [18] used the AFD algorithm to separate lung sounds and heart sounds with different frequencies and proposed a separator based on the AFD algorithm to successfully separate lung sounds and heart sounds. By calculating the kurtosis value of the AFD decomposition component, Liang et al. [19] selected the component that exceeded the set threshold for reconstruction and performed spectrum analysis on the reconstructed signal to extract bearing fault features. In the above method, it is necessary to rely on manual experience to set the estimated signal-to-noise ratio, percentage root–mean-square difference, and other thresholds as the basis for determining the selection of the number of decomposition levels, which may easily lead to overdecomposition or underdecomposition of the signal if it is not properly selected. Literature [20] improved the AFD algorithm in terms of the computational complexity of the algorithm and proposed a Jaya-based AFD method to reduce the computational complexity, but the adaptive criterion of the decomposition level is not clearly given. Therefore, a feature extraction method-based improved adaptive Fourier decomposition (IAFD) and Teager–Kaiser energy operator (TKEO) is applied in rolling bearing fault diagnosis. The key contributions of this paper are as follows:

(1) A combined weight index called SP using percentage root-mean-square difference (PRD) and signal-to-noise ratio (SNR) is constructed, and the whale optimization algorithm is employed to optimize the SP weight parameter.
(2) An IAFD based on optimized SP is presented, where the decomposition levels can be determined adaptively.
(3) A novel feature extraction method-based IAFD and TKEO is proposed, and the effectiveness of the presented method is verified with two data sets.

2. Materials and Methods

2.1. AFD Method. In the complex Hardy space, there is the real number signal $f(t)$, which is transformed into the analytic signal $f(z)$ and decomposed in the $H^2(D)$, including, $D = \{z \in C : |z| < 1\}$, shows the open square circle with the coordinate's origin at its center, C represents the complex plane [21, 22]. Make $f \in H^2(D), f = f_1$, then for any $a_1 \in D$, there is a constant equation as shown in Equation (1).

$$f(z) = \langle f_1, e_{a_1} \rangle e_{a_1}(z) + r_2(z). \tag{1}$$

In Equation (1), $r_2(z)$ is the second-order standard error, which can be expressed as Equation (2).

$$r_2(z) = f_2(z) \frac{z - a_1}{1 - \overline{a}_1 z}. \tag{2}$$

In Equation (2), $f_2(z)$ is the second-order standard error, $\frac{z-a_1}{1-\overline{a}_1 z}$ is a $H^2(D)$ space function with zero point a_1. Equation (3) can be calculated from Equations (1) and (2).

$$f(z) = \langle f_1, e_{a_1} \rangle e_{a_1}(z) + f_2(z) \frac{z - a_1}{1 - \overline{a}_1 z}. \tag{3}$$

Repeat the above steps for f_2 yields Equation (4).

$$f_2(z) = \langle f_2, e_{a_2} \rangle e_{a_2}(z) + f_3(z) \frac{z - a_1}{1 - \overline{a}_1 z}. \tag{4}$$

Equation (5) can be calculated from Equations (3) and (4).

$$\begin{aligned} f(z) = {} & \langle f_1, e_{a_1} \rangle e_{a_1}(z) + \langle f_2, e_{a_2} \rangle e_{a_2}(z) \frac{z - a_1}{1 - \overline{a}_1 z} \\ & + f_3(z) \frac{z - a_1}{1 - \overline{a}_1 z} \frac{z - a_2}{1 - \overline{a}_2 z}. \end{aligned} \tag{5}$$

In Equation (5), a_i is a complex number (inside the open unit circle D), e_{a_i} is the Szegö kernel with a_i orthogonal in D, B_i is the standard rational orthogonal basis, and e_{a_i} is the first factor in B_i.

$$e_{a_i}(z) = \frac{\sqrt{1 - |a_i|^2}}{1 - \overline{a}_i z}, i = 1, 2L, \cdots, nL, \tag{6}$$

$$B_i = \frac{\sqrt{1 - |a_i|^2}}{1 - \overline{a}_i z} \prod_{i=1}^{n} \frac{z - a_i}{1 - \overline{a}_i z}, i = 1, 2L, \cdots, nL. \tag{7}$$

2.2. TKEO Method. TKEO analyzes and tracks signals' energy using a nonlinear energy tracking operator, denoted by φ [23].

Table 1: Single indicators.

Indicators	Formulas	Implication
SNR	$\mathrm{SNR} = 10 \times \log\left(\frac{\sum_{n=1}^{N}(X_s(n)-\overline{X})^2}{\sum_{n=1}^{N}(X_s(n)-X_r(n))^2}\right)$	SNR is the ratio of useful signal to noise signal. It can be used to measure the quality of the signal. Generally speaking, the signal quality is greater the higher the signal-to-noise ratio, where $X_s(n)$ displays the initial signal, $X_r(n)$ symbolizes the signal that was rebuilt, and $\overline{X}$ represents the mean of the original signal
PRD	$\mathrm{PRD}\,(\%) = 100 \times \sqrt{\frac{\sum_{n=1}^{N}(X_s(n)-X_r(n))^2}{\sum_{n=1}^{N}(X_s(n))^2}}$	PRD identifies the variation between the original and recreated signals. The quality of the reconstructed signal often improves with a decreasing root mean square error percentage

$$\varphi[x(t)] = \left[\frac{dx(t)}{dt}\right]^2 - x(t)\frac{d^2x(t)}{dt^2} = [\dot{x}(t)]^2 - x(t)\ddot{x}(t). \tag{8}$$

In Equation (8), $\dot{x}(t)$ and $\ddot{x}(t)$ stand for the first and second order differentials of $x(t)$, respectively. Employing difference in place of differential, then $\varphi[x(n)]$ is defined as Equation (8).

$$j[x(n)] = [x(n)]^2 - x(n-1)x(n+1). \tag{9}$$

In Equation (9), $\varphi[x(n)]$ can be obtained by using three samples to compute the signal energy during any time n. As a result, the transient impact component of the signal can be effectively enhanced by TKEO's output, extract the rolling bearing's early weak fault characteristics.

2.3. Portfolio Weighting Index Construction and Optimization. The selection of the number of traditional AFD decomposition levels lacks the necessary theoretical support and easily leads to overdecomposition or underdecomposition of the signal. Moreover, in the actual acquired signal, the real signal is unknown, which leads to the low accuracy of the evaluation of a single index [17, 24]. To address these limitations, this study combines the strengths of PRD and SNR (as illustrated in Table 1) and introduces a combined weight index [25–28], SP, to enable adaptive selection of AFD decomposition levels.

2.3.1. SP Portfolio Weighting Index Construction. SNR can enhance signal quality and minimize the impact of noise on fault signals, and PRD can assess the divergence between the original and reconstructed signals. Drawing from the construction principles outlined in Sun et al. [29], and to further enhance the index's trend of change, we introduce the combined weight index SP, as shown in Equation (10).

$$\mathrm{SP} = \log_2(1 - a\mathrm{SNR} + b\mathrm{PRD}). \tag{10}$$

Including a and b are greater than 0, which represent the weight coefficients of SNR and PRD, respectively, and $a + b = 1$.

The combined weight index SP is a dimensionless parameter that fully integrates the advantages of SNR and PRD. Equation (10) satisfies that the denoising efficiency and reconstructed signal quality improve with lower SP.

2.3.2. SP Portfolio Weighting Indicator Optimization. To obtain the optimal parameter combination for SP, we employ the whale optimization algorithm (WOA) [30] to optimize the constructed SP weight index. The specific process is outlined as follows:

Step 1: Determining the population size X and randomly generate the position of each whale, parameter initialization settings a, b are 0. Depending on the bearing signal's properties, the parameters of the whale algorithm are: $a_1 = 2$ (initial swimming factor), $b_1 = 3$ (spiral coefficient), whale number N is 30, iteration 100 times.

Step 2: According to the optimization objective function $\mathrm{minSP} = \log_2(1 - a\mathrm{SNR} + b\mathrm{PRD})$, identify the individual with the greatest value for fitness by computing their value.

Step 3: Enter the main loop; the value of a_1 drops from 2 to 0. Including, the random number $p \in [0, 1]$, A is a random value in $[-a_1, a_1]$. If $p < 0.5$ and $|A| < 1$, the whale updates its position by swinging; otherwise, the individual position is randomly updated. If $p \geq 0.5$, the whale updates position in spiral mode.

Step 4: Reevaluate whale populations to find the best individual and location.

Step 5: The loop ends if the stop target is satisfied; otherwise, move on to Step 2 and continue the loop.

Step 6: Output the global optimal solution.

3. The Proposed Method

The overall IAFD bearing fault feature extraction approach is depicted in Figure 1. These are the precise steps:

Step 1: Parameter initialization, decomposition level $N = 1$, $\mathrm{SP} = \infty$. The traditional AFD is used to decompose the vibration signal into several individual components and a residual component, r.

Step 2: The individual components obtained from Step 1 are reconstructed by adding all the individual components together.

Step 3: Calculating the PRD and SNR of each individual component separately.

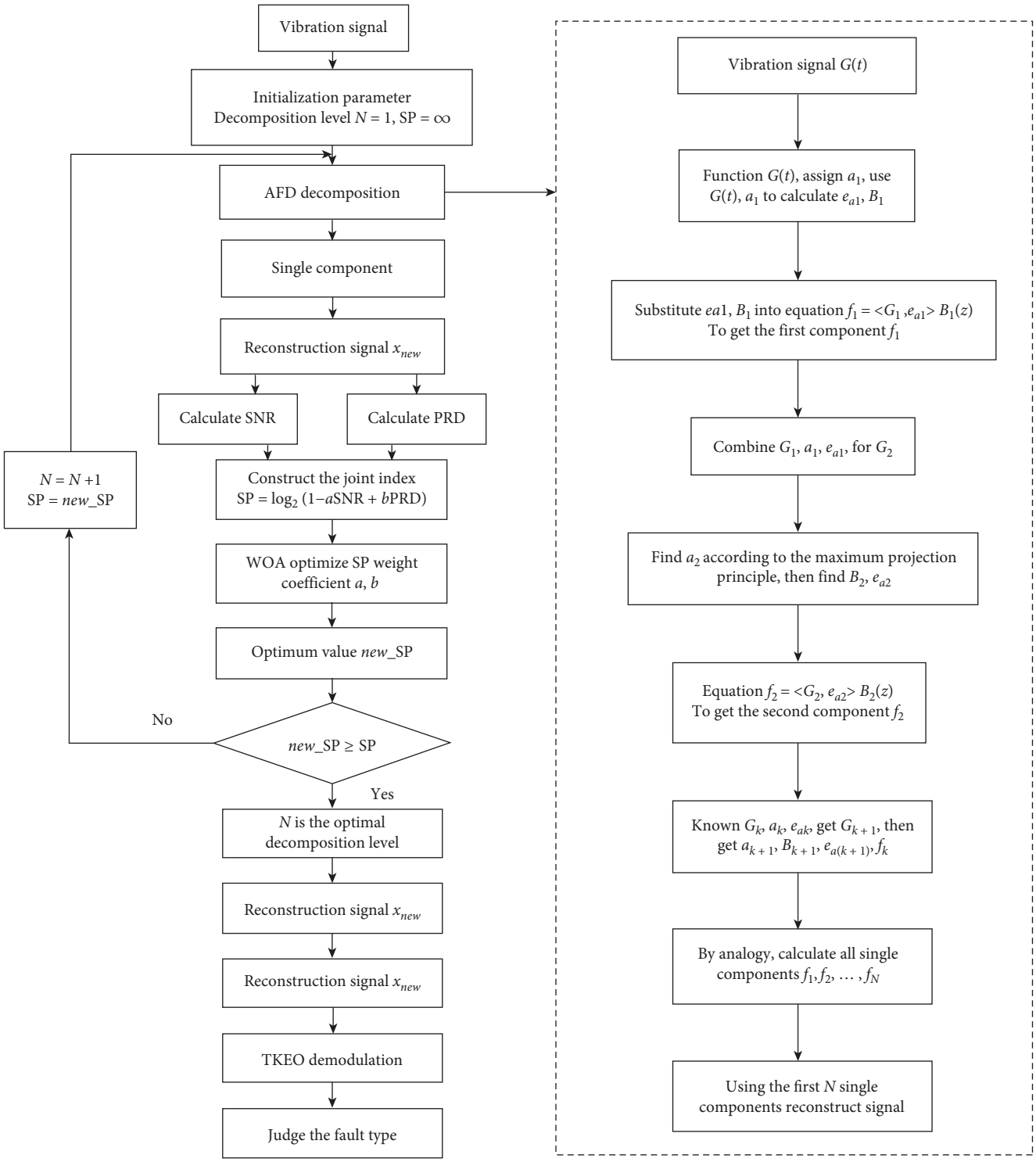

Figure 1: IAFD and TKEO-based rolling bearing defect feature extraction.

$$\mathrm{PRD}\ (\%) = 100 \times \sqrt{\frac{\sum_{n=1}^{N} (X_s(n) - X_r(n))^2}{\sum_{n=1}^{N} (X_s(n))^2}}, \quad \mathrm{SNR} = 10 \times \log\left(\frac{\sum_{n=1}^{N} \left(X_s(n) - \overline{X}\right)^2}{\sum_{n=1}^{N} (X_s(n) - X_r(n))^2}\right). \tag{11}$$

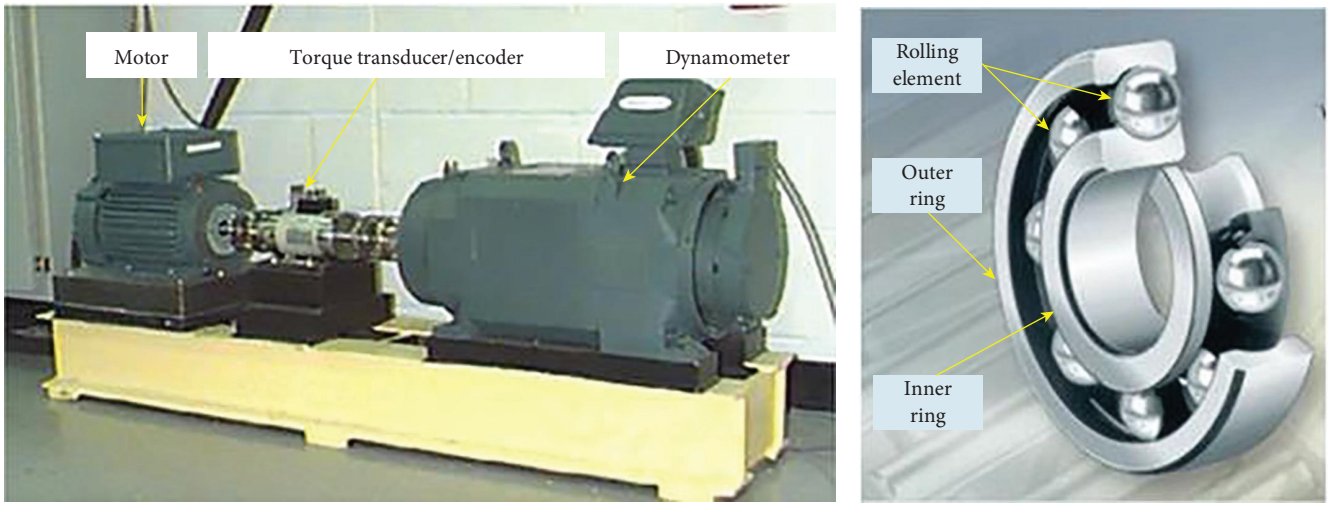

Figure 2: Bearing experiment platform of CWRU.

Table 2: Parameters of deep groove ball bearing.

Model	Number of scrolling bodies (Z)	Inner ring diameter (mm)	Outer ring diameter (mm)	Contact angle (θ)	Rolling body diameter (mm)	Nodal diameter (mm)	Motor speed (rpm)
6205-2RS JEM SKF	9	25	52	0°	7.94	39.04	1,797

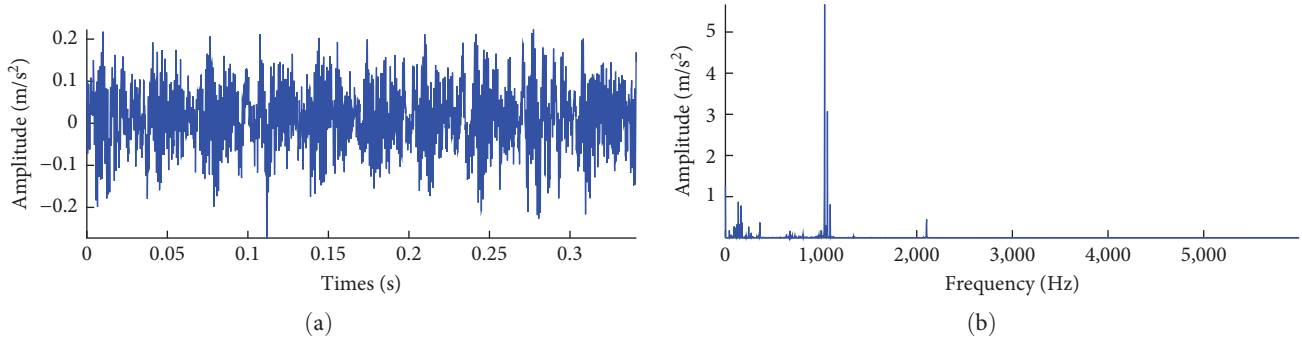

Figure 3: Time domain and frequency domain waveform of normal signal: (a) time domain waveforms; (b) frequency domain waveform.

Step 4: Construct a joint index SP using the calculated PRD and SNR, $\mathrm{SP} = \log_2(1 - a\mathrm{SNR} + b\mathrm{PRD})$.

Step 5: Using the WOA to optimize the weighting coefficients a and b for SP. Based on the characteristics of the bearing signal, set the parameters of the whale algorithm as follows: $a_1 = 2$ (initial swimming factor), $b_1 = 3$ (spiral coefficient), $N = 30$ (number of whales), and perform 100 iterations. Obtain the optimal weighting coefficients and calculate the joint index *new*_SP.

Step 6: Compare *new*_SP and SP; if *new*_SP $\geq$ SP, then N is the optimal decomposition layer; otherwise, *new*_SP value is assigned to SP, $N = N + 1$, and Step 6 is repeated until the optimal decomposition layer N is found.

Step 7: The decomposed first N single components are recombined, and the recombined signal is demodulated by TKEO. The feature frequency is extracted according to the demodulated signal to judge the fault.

4. Experimental and Comparative Analysis

4.1. Case 1: Case Western Reserve University (CWRU) Data Analysis. This approach is tested and validated using data obtained from the inner and outer rings of bearings provided by CWRU [31]. Figure 2 and Table 2 depict the bearing test platform and relevant bearing parameters. The analyzed data have a sampling frequency of 12 kHz and a data length of 4,096. Based on Table 2 and the principles of rolling bearing vibration theory [32], the characteristic frequencies of inner and outer ring faults are calculated as follows: BPFI = 162.185 Hz and BPFO = 107.305 Hz, respectively.

4.1.1. Outer Ring Fault Signal Analysis. Figures 3 and 4 depict the bearing's time-domain and frequency-domain waveforms under fault-free and normal operating conditions. Figure 4 shows how it compares to the regular working state.

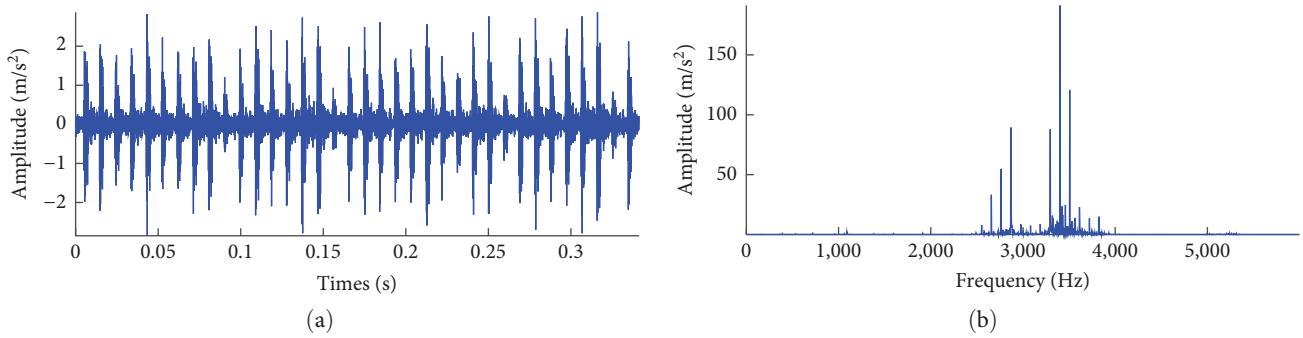

(a) (b)

Figure 4: Time domain and frequency domain waveform of fault signal: (a) time domain waveforms; (b) frequency domain waveform.

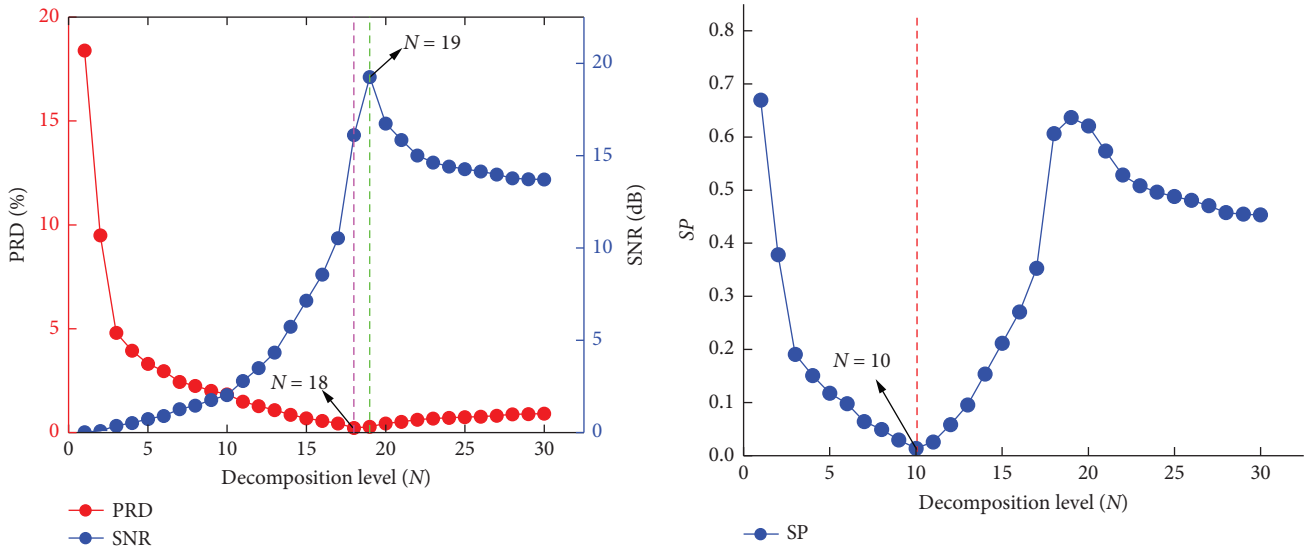

(a) (b)

Figure 5: Changes of single index and combined index SP with the number of decomposition layers for rolling bearing outer ring faults.

The fault state's time domain waveform clearly exhibits a periodic pulse fluctuation law, and the abnormal component appears in the frequency domain waveform, which can preliminarily determine that the bearing has failed. But only through this phenomenon cannot get the specific fault type and location of the rolling bearing; the signal needs further analysis and processing to determine the fault type. So, IAFD is utilized to break down the bearing vibration signal.

When the optimal decomposition level is obtained by WOA, the SP weight coefficient is $a = 0.51$ and $b = 0.49$. As shown in Figure 5, the number of decomposition levels affects both the single index and the combined index. The optimal decomposition levels of AFD are determined according to SP, PRD, and SNR, respectively. In order to keep track of the index's change trend, when the optimal decomposition levels appear, the decomposition is continued to 30 levels. Figure 5 shows that the joint index SP determined that there are 10 breakdown levels. But only 18–19 breakdown levels are identified by a single index. The fault signal is further decomposed by AFD.

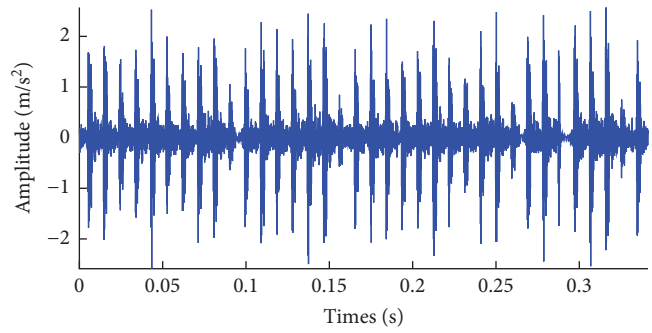

Figure 6: Reconstructed signal.

Whenever there are 10 decomposition levels, the reconstructed signal x_{new} is shown in Figure 6. The recovered signal x_{new} is modulated using TKEO, and the resulting TKEO spectrum is shown in Figure 7(a). From Figure 7(a), there is a significant peak phenomenon at 105.5 Hz, in proximity to the bearing outer ring fault's theoretical value of 107.305

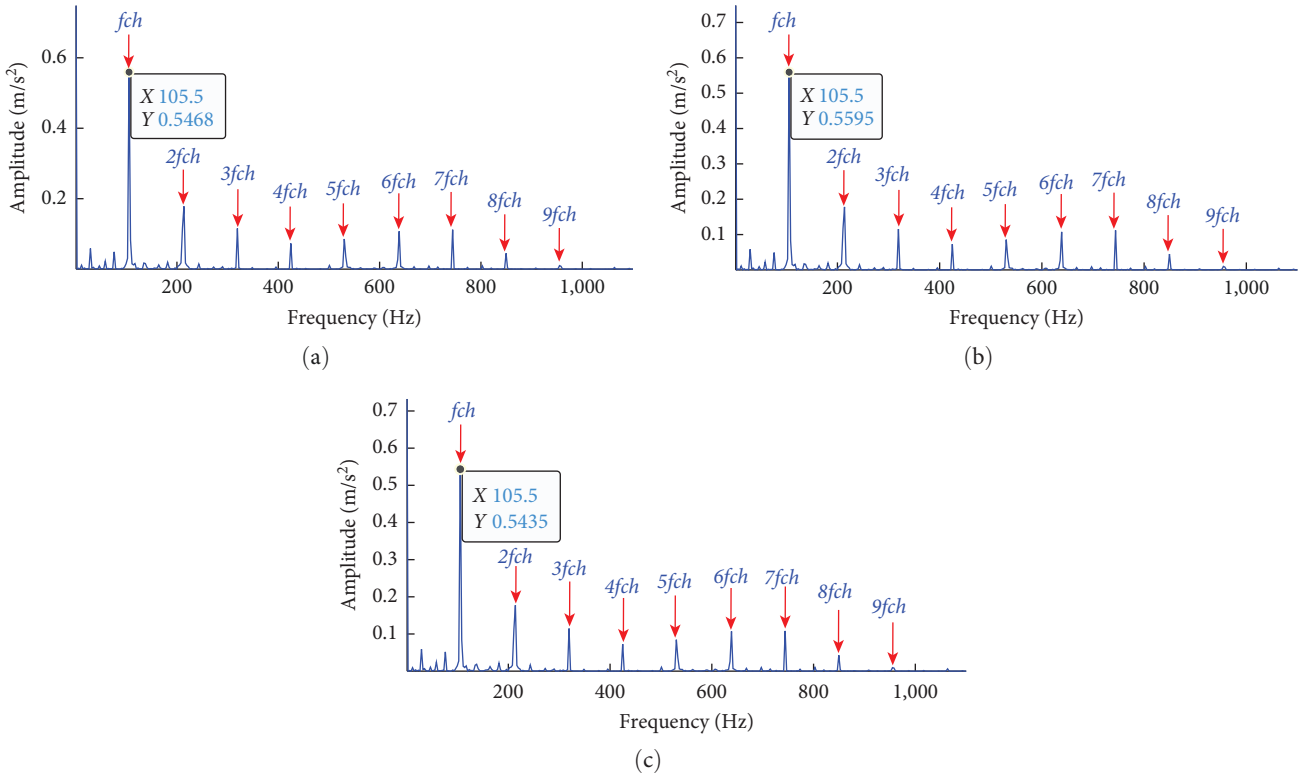

Figure 7: Teager–Kaiser energy operator spectrum: (a) SP (10 levels); (b) PRD (18 levels); (c) SNR (19 levels).

Table 3: Comparison of running time of outer ring failure of rolling bearings.

Category	SP + WOA	PRD	SNR
Running time (s)	**1.9223**	3.7964	3.9032

Bold value emphasizes that the calculation time of our method is lower.

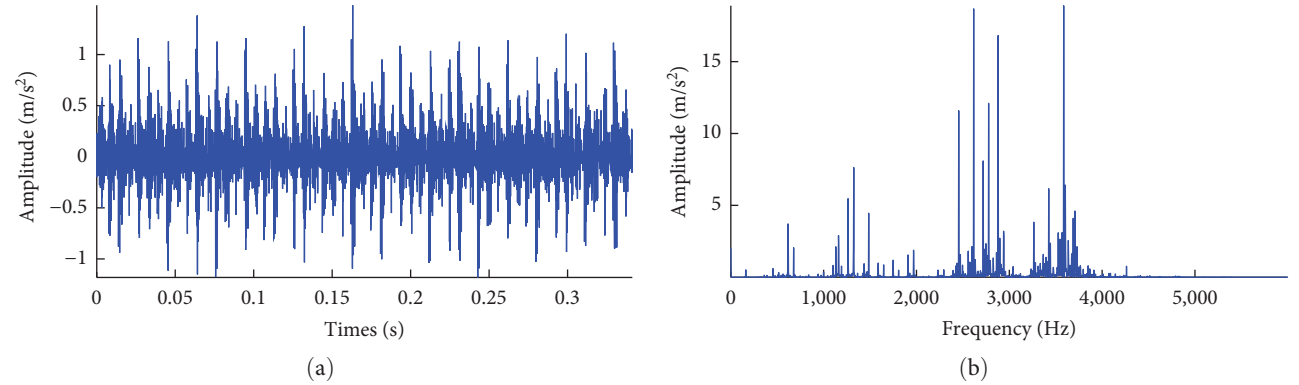

Figure 8: Time domain and frequency domain waveform of fault signal: (a) time domain waveforms; (b) frequency domain waveform.

Hz, and we can clearly observe the 2–10 times the peak frequency. As a result, it is possible to conclude that the bearing has an outer ring flaw. When the number of decomposition levels is 18 and 19, the obtained TKEO spectrum is shown in Figures 7(b) and 7(c). The comparative analysis shows that the decomposition layer $N = 10$ can obtain excellent performance. At the same time, Table 3 compares the operating efficiency of different indicators, and the operating efficiency of the proposed method is improved by 49.4% and 50.8%, respectively. In summary, the proposed method takes into account both fault diagnosis performance and operating efficiency and has strong practicability.

4.1.2. Inner Ring Fault Signal Analysis. The time–frequency and frequency-domain waveforms of the inner ring fault signal are shown in Figure 8. Similarly, consistent with the

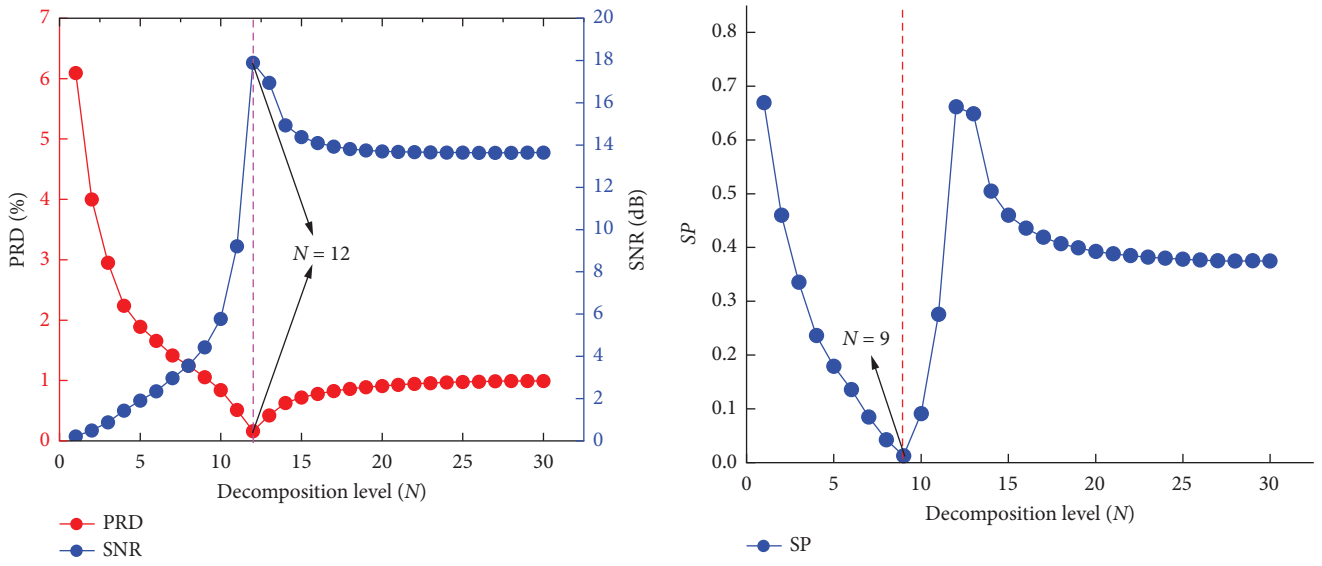

FIGURE 9: Changes of single index and combined index SP with the number of decomposition layers for rolling bearing inner ring faults.

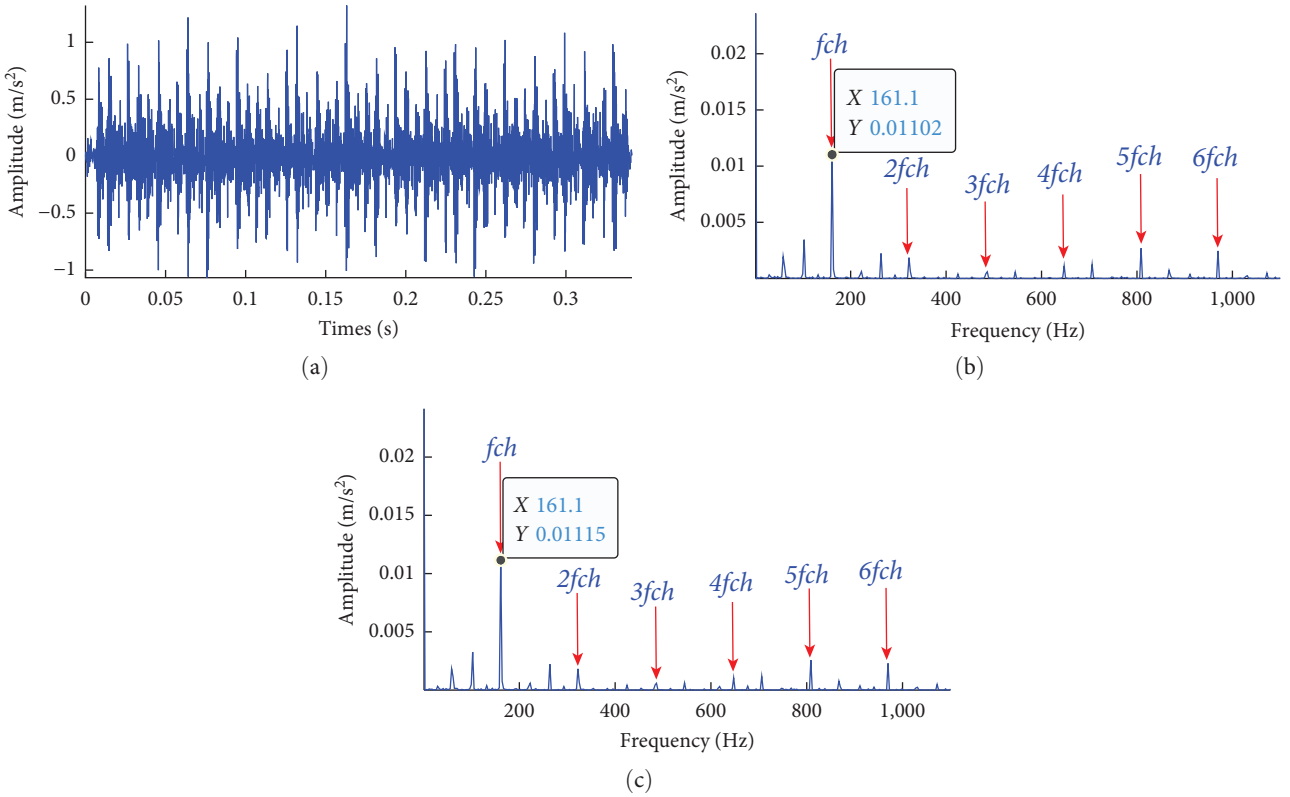

FIGURE 10: Reconstructed signal and Teager–Kaiser energy operator spectrum: (a) reconstructed signal; (b) SP (9 levels); (c) PRD and SNR (12 levels).

outer ring fault, only the bearing fault can be determined, but detailed information such as the type of fault cannot be obtained, and then IAFD is used to decompose the fault signal of the bearing.

Using WOA to optimize the parameters of the combined index SP, the parameter settings match those used in the bearing outer ring experiment. When the optimal decomposition level is obtained by WOA, the weight coefficients

Table 4: Comparison of running time of inner ring failure of rolling bearings.

Category	SP + WOA	PRD	SNR
Running time (s)	**1.6128**	2.3157	2.3157

Bold value emphasizes that the calculation time of our method is lower.

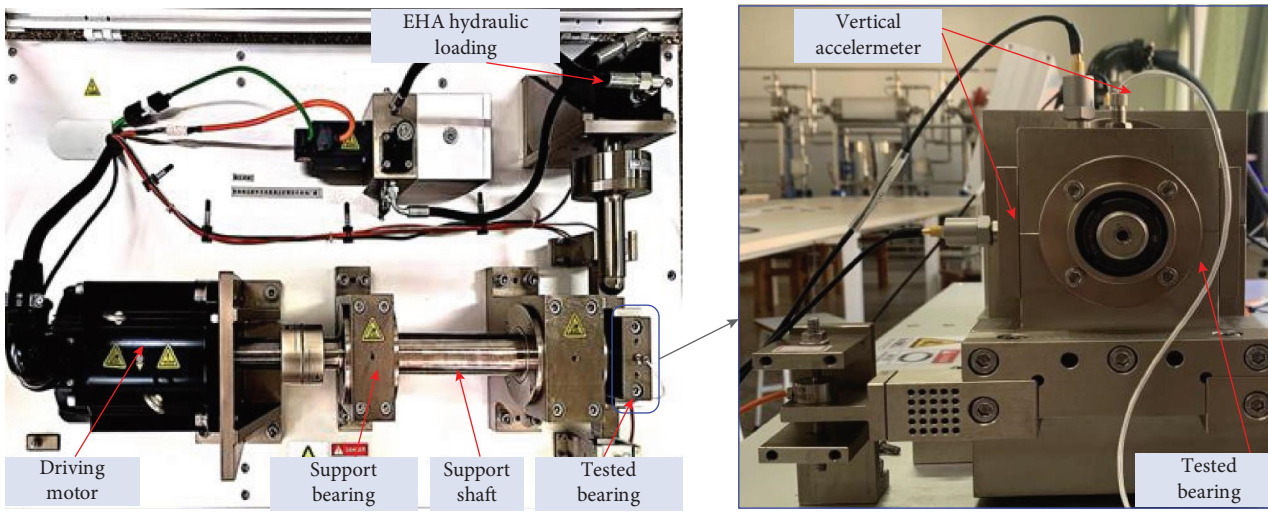

Figure 11: Bearing experiment platform of KUST-SY.

Table 5: Parameters of bearing.

Model	Number of scrolling bodies (Z)	Contact angle (θ)	Outer ring diameter (mm)	Inner ring diameter (mm)	Rolling body diameter (mm)	Motor speed (rpm)	Rated dynamic load (KN)
6205-2RSJEM SKF	9	0	39.80	29.30	7.9	1,797	12.82

$a = 0.38$ and $b = 0.62$. Figure 9 shows the variation of the single index and joint index with the number of decomposition levels. According to SP, PRD, and SNR, the optimal decomposition levels of AFD are determined to be 9, 12, and 12, respectively, which are abbreviated as [9, 12]. Figure 10 displays the reconstructed signal x_{new} and its TKEO spectrum corresponding to the ideal decomposition level, and the operating efficiency statistics are shown in Table 4. Figure 10 shows a distinct peak phenomenon at 161.1 Hz, which is near the theoretical value of the bearing inner ring fault (162.185 Hz) and can be clearly observed as 2–6 times the peak. As a result, it is possible to conclude that the bearing has an inner ring fault. The effectiveness and viability of the suggested strategy are further confirmed by comparing statistics and tables.

4.2. Laboratory Self-Made Bearing Platform Data Analysis and Validation. For IAFD analysis and verification, the real test data of the KUST-SY bearing platform built by the lab is used. This is done to confirm that the suggested method works. The platform can model various rolling bearing failure scenarios. Figure 11 is the KUST-SY bearing experimental platform, which is composed of a drive motor, shaft, support bearing seat, EHA hydraulic loading system, acceleration sensor, and measured bearing.

In this experiment, considering the existing experimental conditions, the inner and outer rings of the bearing's fault operating circumstances are primarily simulated. A laser cutter is used to create surface cracks in the inner and outer rings (fault diameter 0.2 mm). The specific parameters are as follows: Sampling frequency: 25.6 kHz; sampling interval: 20 s; sampling time: 10 s. The bearing under test is 6205-2RSJEM SKF, with parameters listed in Table 5. According to Wang et al. [21], the inner ring fault characteristic frequency is BPFI = 162.33 Hz, and BPFO = 107.22 Hz for the outer ring fault.

The effectiveness and feasibility of the proposed method are vitrificated using the outer ring and inner ring data sets, which are collected in the horizontal direction, respectively, and the number of sampling points is 4,096. The comparative experimental analysis results are as follows:

(1) The optimal layer number of the proposed method is shown in Figures 12 and 13 based on SP, PRD, and SNR. It can be seen from Figure 12 that the number of optimal decomposition layers is 3 selected by SP, but the number of optimal decomposition layers is 5 selected by a single PRD or SNR in the condition of an outer ring fault. Similarly, the number of optimal

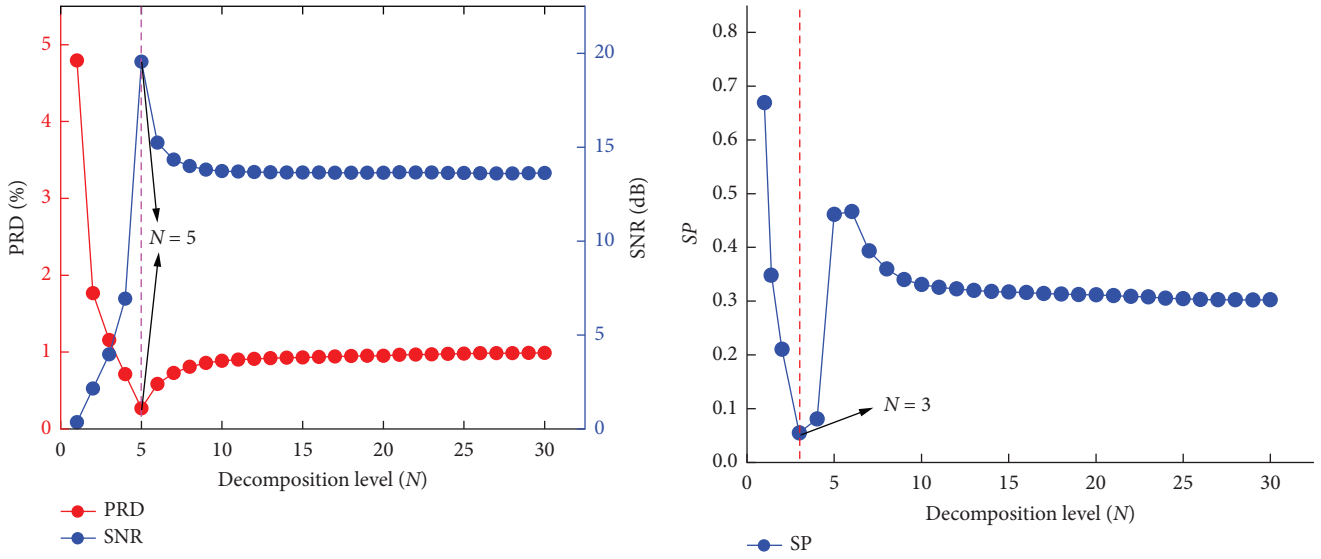

Figure 12: Variation curve of index with the number of decomposition levels in case of outer ring failure: (a) variation of a single indicator with the number of decomposition levels; (b) variation of joint index SP with the number of decomposition levels.

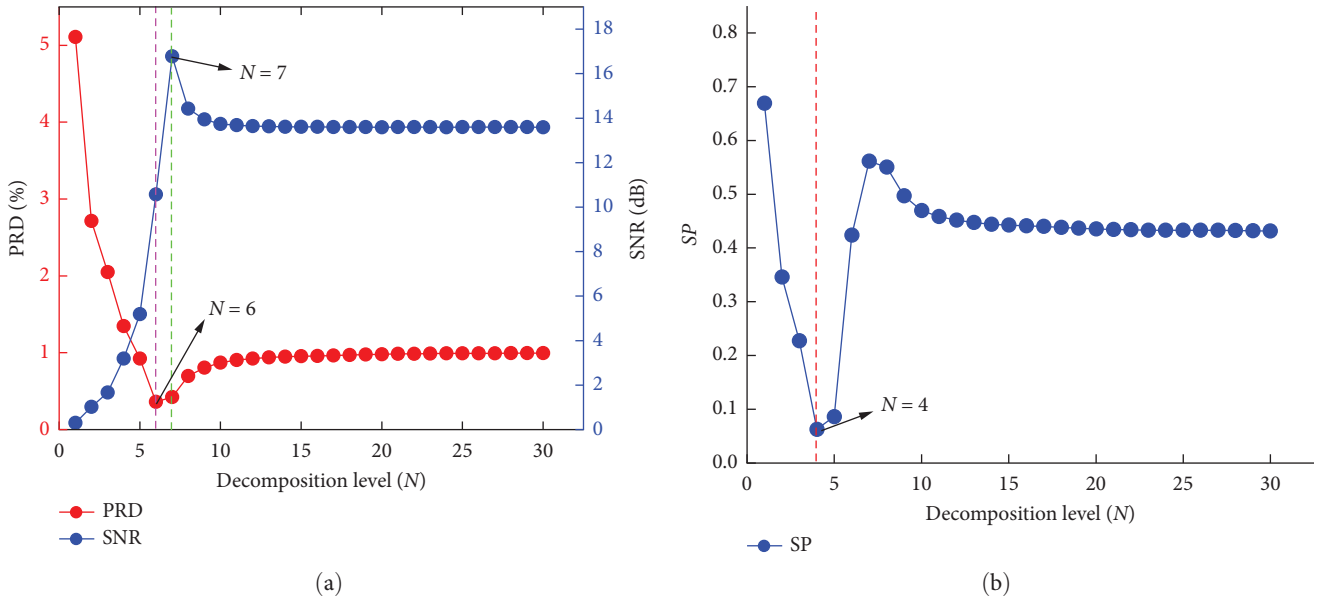

Figure 13: Variation curve of index with the number of decomposition levels in case of inner ring failure: (a) variation of a single indicator with the number of decomposition levels; (b) variation of joint index SP with the number of decomposition levels.

decomposition layers [4, 6, 7] of the inner ring fault is calculated by SP, PRD, and SNR.

(2) The TKEO spectrum of the reconstructed signal x_{new} is extracted and illustrated in Figures 14 and 15. Then, the characteristic frequency of the outer and inner rings is extracted by the TKEO spectrum. Additionally, the consuming time of comparative methods is counted and displayed in Table 6. It can be intuitively seen that the proposed method takes the shortest time, which also further proves the effectiveness and feasibility of the presented method.

5. Discussion

The number of decomposition levels is preset manually for the typical AFD, which, if incorrectly chosen, could result in either an over- or underdecomposition of the signal. Therefore, in this paper, we fuze two single indicators, root mean square error percentage and signal-to-noise ratio, and create a joint indicator SP to calculate the AFD's adaptive decomposition's number of levels. The adaptive selection of AFD decomposition levels is realized, which effectively avoids the mis-decomposition of signals due to artificially set decomposition levels, and this enhances the ability of AFD to decompose signals and identify faults.

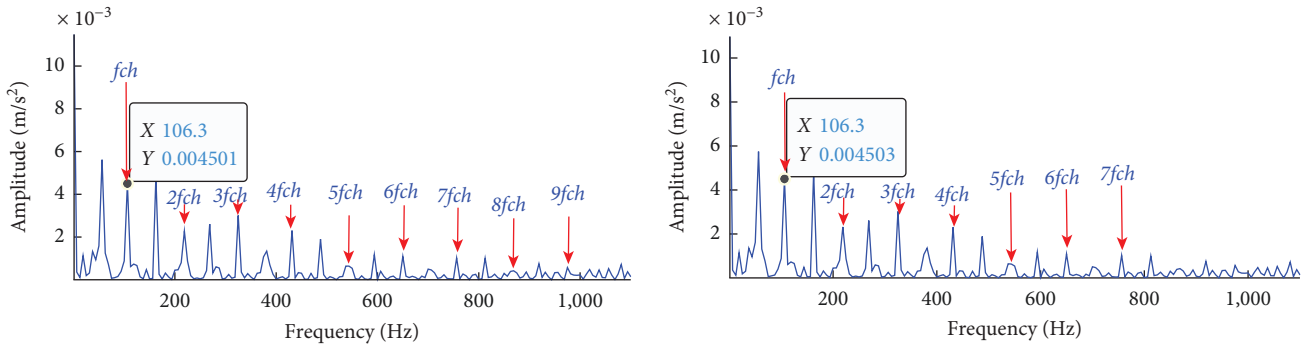

Figure 14: Teager–Kaiser energy operator spectrum: (a) SP (3 levels); (b) PRD and SNR (5 levels).

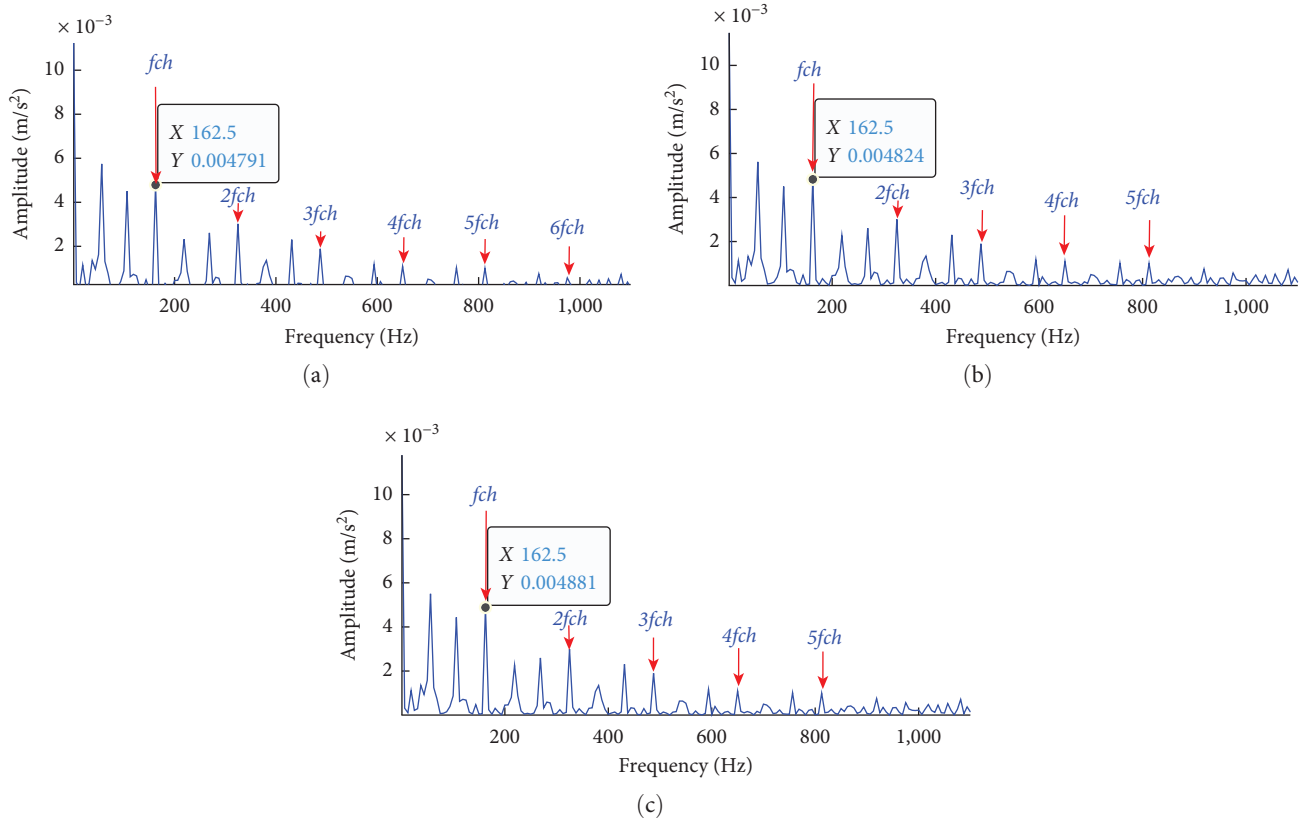

Figure 15: Teager–Kaiser energy operator spectrum: (a) SP (4 levels); (b) PRD (6 levels); (c) SNR (7 levels).

Table 6: Operation time comparison.

Category	SP + WOA	PRD	SNR
Outer ring failure running time (s)	**0.7964**	1.3032	1.3032
Inner ring failure running time (s)	**0.9964**	1.5607	1.6015

Bold values emphasize that the calculation time of our method is lower.

6. Conclusions

This paper introduces a weight index SP, which combines the PRD and SNR for the adaptive selection decomposition levels of the AFD method. The proposed method is validated using vibration data from the inner and outer rings of bearings on the CWRU platform and the KUST-SY experimental platform. We can obtain some useful conclusions through the experiment.

(1) The decomposition level of AFD can be adaptively selected by the constructed joint index SP. It can effectively avoid the misclassification of signals caused by artificially set.

(2) The proposed IAFD provides a new method for fault diagnosis of bearings, which improves the theoretical basis for adaptive determination of AFD decomposition

levels, enhances the performance of AFD in signal decomposition and fault diagnosis, and reduces the waste of computing resources.

(3) The proposed method has achieved signal adaptive decomposition and feature extraction. Furthermore, the performance degradation evaluation theory and methods of composite fault and health management for rolling bearings will be further researched.

Data Availability

The data used to support this research are available from the corresponding author upon request.

Conflicts of Interest

The authors declare that they have no known competing financial interests or personal relationships that could have appeared to influence the work reported in this paper.

Acknowledgments

The contributions of all my co-authors are gratefully acknowledged. Moreover, this manuscript is supported by the National Natural Science Foundation of China (nos. 62163020 and 62173168) and the Science & Research Program of Yunnan Province (202102AD080007 and 202101BE070001-055).

References

[1] H. Pu, K. Zhang, and Y. An, "Restricted sparse networks for rolling bearing fault diagnosis," *IEEE Transactions on Industrial Informatics*, vol. 19, no. 11, pp. 11139–11149, 2023.

[2] B. Chen, W. Zhang, J. Xi Gu et al., "Product envelope spectrum optimization-gram: an enhanced envelope analysis for rolling bearing fault diagnosis," *Mechanical Systems and Signal Processing*, vol. 193, Article ID 110270, 2023.

[3] C. Huo, Q. Jiang, Y. Shen, Q. Zhu, and Q. Zhang, "Enhanced transfer learning method for rolling bearing fault diagnosis based on linear superposition network," *Engineering Applications of Artificial Intelligence*, vol. 121, Article ID 105970, 2023.

[4] P. Yin, J. Nie, X. Liang et al., "A multiscale graph convolutional neural network framework for fault diagnosis of rolling bearing," *IEEE Transactions on Instrumentation and Measurement*, vol. 72, pp. 1–13, 2023.

[5] S. B. Xia, J. Z. Zhang, S. C. Xu, and L. Y. Zhang, "The present situation and prospect of rotating machinery fault diagnosis technology," *Journal of Vibration and Shock*, no. 2, pp. 5–9+96, 1997.

[6] F. T. Wang, G. Deng, H. T. Wang, X. G. Yu, Q. K. Han, and H. K. Li, "Fault diagnosis of rolling bearing based on EMD and SSAE," *Journal of Vibration Engineering*, vol. 32, no. 2, pp. 368–376, 2019.

[7] Z. Dang, Y. Lv, Y. Li, and G. Wei, "Improved dynamic mode decomposition and its application to fault diagnosis of rolling bearing," *Sensors*, vol. 18, no. 6, Article ID 1972, 2018.

[8] W. S. Su, F. T. Wang, Z. X. Zhang, Z. G. Guo, and H. K. Li, "Application of EMD denoising and spectral kurtosis in early fault diagnosis of rolling element bearings," *Journal of Vibration & Shock*, vol. 29, no. 3, pp. 18–21, 2010.

[9] R. Tong, J. S. Kang, B. C. Li, and W. Zhong, "Gear fault feature extraction based on LCD and Bispectrum analysis," *Journal of Academy of Armored Forces Engineering*, vol. 32, no. 5, pp. 46–52, 2018.

[10] Z. T. Wu, J. S. Cheng, and B. Q. Li, "Local characteristic-scale decomposition method based on differential operator and its application," *China Mechanical Engineering*, vol. 26, no. 17, pp. 2290–2296, 2015.

[11] J. S. Smith, "The local mean decomposition and its application to EEG perception data," *Journal of the Royal Society, Interface*, vol. 2, no. 5, pp. 443–454, 2005.

[12] J. S. Cheng, Y. Yang, and Y. Yang, "Local characteristic scale decomposition method and its application in gear fault diagnosis," *Journal of Mechanical Engineering*, vol. 48, no. 9, pp. 64–71, 2012.

[13] J. S. Cheng, J. D. Zheng, and Y. Yang, "A non-stationary signal analysis approach—the local characteristic scale decomposition method," *Journal of Vibration Engineering*, vol. 25, no. 5, pp. 215–220, 2012.

[14] Z. T. Wu, J. S. Cheng, and G. X. Zhang, "Newton interpolation based local characteristic-scale de-composition method and its application," *Journal of Electronic Measurement & Instrumentation*, vol. 29, no. 9, pp. 1348–1355, 2015.

[15] Z. T. Wu, J. S. Cheng, and B. Q. Li, "The method of generalized local characteristic-scale de-composition and its application," *Journal of Vibration Engineering*, vol. 29, no. 2, pp. 331–339, 2016.

[16] T. Qian, L. M. Zhang, and Z. X. Li, "Algorithm of adaptive Fourier decomposition," *IEEE Transactions on Signal Processing*, vol. 59, no. 12, pp. 5899–5906, 2011.

[17] Z. Wang, F. Wan, C. M. Wong, and L. Zhang, "Adaptive Fourier decomposition based ECG denoising," *Computers in Biology and Medicine*, vol. 77, pp. 195–205, 2016.

[18] Z. Wang, J. Nuno da Cruz, and F. Wan, "Adaptive Fourier decomposition approach for lung-heart sound separation," in *2015 IEEE International Conference on Computational Intelligence and Virtual Environments for Measurement Systems and Applications (CIVEMSA)*, IEEE, Shenzhen, China, June 2015.

[19] Y. Liang, L. M. Jia, G. Q. Cai, and J. C. Liu, "AFD algorithm based rolling bearing fault diagnosis method," *China Railway Science*, vol. 34, no. 1, pp. 95–100, 2013.

[20] A. Kirkbas, A. Kizilkaya, and E. Bogar, "Optimal basis pursuit based on Jaya optimization for adaptive Fourier decomposition," in *2017 40th International Conference on Telecommunications and Signal Processing (TSP)*, pp. 538–543, IEEE, Barcelona, Spain, July 2017.

[21] Z. Wang, C. M. Wong, A. Rosa, T. Qian, and F. Wan, "Adaptive Fourier decomposition for multi-channel signal analysis," *IEEE Transactions on Signal Processing*, vol. 70, pp. 903–918, 2022.

[22] Z. Wang, L. M. Yang, C. M. Wong, and F. Wan, "Fast basis searching method of adaptive Fourier decomposition based on Nelder-Mead algorithm for ECG signals," *Advances in Neural Networks*, vol. 9377, pp. 305–314, 2015.

[23] J. Ma, J. Wu, and X. Wang, "Incipient fault feature extraction of rolling bearings based on the MVMD and Teager energy operator," *ISA Transactions*, vol. 80, pp. 297–311, 2018.

[24] G. H. Qin, J. Gao, H. C. Ye, G. J. Jiang, S. Huang, and X. C. Lai, "Tool wear prediction based on fused evaluation metrics and neural networks," *Acta Armamentarii*, vol. 42, no. 9, pp. 2013–2023, 2021.

[25] C. Tan, L. Zhang, and H. T. Wu, "A novel Blaschke unwinding adaptive-Fourier-decomposition-based signal compression algorithm with application on ECG signals," *IEEE Journal of*

Biomedical and Health Informatics, vol. 23, no. 2, pp. 672–682, 2019.

[26] J. G. Jiang and Q. Wang, "Fault diagnosis of motor bearings based on MEEMD and cliff-correlation coefficient," *Techniques of Automation and Applications*, vol. 37, no. 1, pp. 65–70, 2018.

[27] W. C. Cui, A. Q. Xu, W. Li, and F. L. Meng, "Gear fault diagnosis based on local characteristic—scale decomposition and instantaneous frequency spectrum," *Computer Measurement & Control*, vol. 24, no. 3, pp. 29–32, 2016.

[28] L. M. Zhu and W. C. Cui, "Weicheng bearing fault diagnosis based on local feature scale decomposition and basic scale entropy," *Journal of Mechanical Transmission*, vol. 41, no. 9, pp. 183–188, 2017.

[29] P. Sun, Y. Liao, and J. Lin, "The shock pulse index and its application in the fault diagnosis of rolling element bearings," *Sensors*, vol. 17, no. 3, Article ID 535, 2017.

[30] S. Mirjalili and A. Lewis, "The whale optimization algorithm," *Advances in Engineering Software*, vol. 95, pp. 51–67, 2016.

[31] K. Loparo and B. S. Bang, "Bearings Vibration Data Set," Case Western Reserve University, https://engineering.case.edu/bearingdatacenter/download-data-file.

[32] X. Y. Yang, W. Q. Deng, and J. Ma, "Fault diagnosis of rolling bearings based on IRCMNDE and NNCHC," *Journal of Aerospace Power*, vol. 37, no. 6, pp. 1150–1161, 2022.